Genetic Analyses of Epigenetic Predictors that Estimate Aging, Metabolic Traits, and Lifespan

Khyobeni Mozhui [1, 2*], Ake T. Lu[3], Caesar Z Li [3], Amin Haghani [4], Jose Vladimir Sandoval-Sierra [1], Robert W. Williams [2], Steve Horvath[3, 4]

[1] Department of Preventive Medicine, University of Tennessee Health Science Center, College of Medicine, Memphis, Tennessee, USA

[2] Department of Genetics, Genomics and Informatics, University of Tennessee Health Science Center, College of Medicine, Memphis, Tennessee, USA

[3] Department of Human Genetics, David Geffen School of Medicine, University of California Los Angeles, Los Angeles, CA, USA

[4] Department of Biostatistics, Fielding School of Public Health, University of California Los Angeles, Los Angeles, CA, USA

[*]Correspondence:
Khyobeni Mozhui
kmozhui@uthsc.edu

Abstract

DNA methylation (DNAm) clocks are accurate molecular biomarkers of aging. However, the clock mechanisms remain unclear. Here, we used a pan-mammalian microarray to assay DNAm in liver from 339 predominantly female mice belonging to the BXD family. We computed epigenetic clocks and maximum lifespan predictor (predicted-maxLS), and examined associations with DNAm entropy, diet, weight, metabolic traits, and genetic variation. The epigenetic age acceleration (EAA) derived from the clocks, and predicted-maxLS were correlated with lifespan of the BXD strains. Quantitative trait locus (QTL) analyses uncovered significant QTLs on chromosome (Chr) 11 that encompasses the *Erbb2/Her2* oncogenic region, and on Chr19 that contains a cytochrome P450 cluster. Both loci harbor candidate genes associated with EAA in humans (*STXBP4*, *NKX2*-3, *CUTC)*. Transcriptome and proteome analyses revealed enrichment in oxidation-reduction, metabolic, and mitotic genes. Our results highlight loci that are concordant in human and mouse, and demonstrate intimate links between metabolism, body weight, and epigenetic aging.

Keywords: epigenetic clock, lifespan, aging, DNA methylation, QTL, weight, diet

Introduction

Epigenetic clocks are widely used molecular biomarkers of aging[1]. These biological clocks are based on the methylation status across an ensemble of "clock CpGs" that are collectively used to derive a DNA methylation (DNAm) based estimate of age (DNAmAge). This estimate tracks closely, but not perfectly, with an individual's chronological age. How much the DNAmAge deviates from the known chronological age is a measure of the rate of biological aging. Denoted as epigenetic age acceleration (EAA), a more accelerated measure (positive EAA) suggests an older biological age. While DNAmAge predicts age, its age-adjusted counterpart, EAA, is associated with health, fitness, exposure to stressors, body mass index (BMI), and even life expectancy[2-6].

DNAm clocks were initially reported for humans[7,8]. Since then, the age estimator has been extended to model organisms[9-11], and different variants of human clocks have also been developed. Some clocks are tissue specific, others are pan-tissue, and others perform well at predicting health and life expectancy[5,8,12-14].

A new microarray platform was recently developed to profile CpGs that have high conservation across mammalian clades. This pan-mammalian DNAm array (HorvathMammalMethylChip40) provides a common platform to measure DNAm, and has been used to build universal epigenetic clocks that can estimate age across a variety of tissues and mammalian species[15,16]. Another remarkable development with this array is the novel lifespan predictor that can estimate the maximum lifespan of over 190 mammals at high accuracy[17].

Here, we examine these novel clocks, lifespan predictor, and methylome entropy in a cohort of mice belonging to the BXD family that were maintained on either normal chow or high-fat diet (HFD)[18,19]. The BXDs are a well-established mouse genetic reference panel that were first created as a family of recombinant inbred (RI) strains by crossing two inbred progenitors: C57BL/6J (B6) and DBA/2J (D2). The family has been expanded to ~150 fully sequenced progeny strains[20,21]. Members of the BXD family vary greatly in their metabolic profiles, aging rates, and natural life expectancy[18,19,22-24]. The genetic variation, and the availability of accompanying deep -omic data make the BXDs a unique experimental population for dissecting the genetic modulators of epigenetic aging. Previously, we explored the aging methylome in a small number of BXD cases and found that HFD and higher body weight were associated with higher age-dependent changes in methylation[25]. In the present work, our goals were to (1) test the accuracy of the DNAm measures in predicting age, lifespan, and association with diet and metabolic characteristics, and (2) apply quantitative trait locus (QTL) mapping and gene expression analyses to uncover loci and genes that contribute to these DNAm biomarkers.

Our results are consistent with a faster clock for cases on HFD, and with higher body weight. Both the DNAmAge and lifespan predictors were correlated with the genotype-dependent life expectancy of female BXDs. We report QTLs on chromosomes (Chrs) 11 and 19. A strong candidate gene in the chromosome (Chr) 11 interval (referred to as *Eaaq11*) is *Stxbp4*, a gene that has been consistently associated with EAA by human genome-wide association studies (GWAS)[26-28]. The Chr19 QTL (*Eaaq19*) also harbors strong contenders including *Cyp26a1*, *Myof*, *Cutc*, and *Nkx2–3*, and the conserved genes in humans have been associated with longevity and

EAA[28-30]. *Eaaq19* may also have an effect on body weight change with age. We performed gene expression analyses to clarify the physiology associated with the DNAm traits, and this, perhaps unsurprisingly, highlighted metabolic networks as strong expression correlates of epigenetic aging.

Results

Description of samples

The present study uses liver DNAm data from 339 predominantly female mice (18 males only) belonging to 45 isogenic members of the BXD family, including F1 hybrids, and both parental strains. Age ranged from 5.6 to 33.4 months. Mice were all weaned onto a normal chow (control diet; CD) and a balanced subset of cases were then randomly assigned to the HFD (see Roy et al for details [18]). Tissues were collected at approximately six months intervals (see Williams et al. [19]). Individual-level data of cases used in this study are in **Data S1**.

Correlation with chronological age

For biological age prediction, three different types of mouse DNAm clocks were computed, each as a pair: liver-specific, and pan-tissue (**Table 1**). These are: (1) a general DNAm clock (referred to simply as DNAmAge): clock trained without pre-selecting for any specific CpG subsets; (2) developmental clock (dev.DNAmAge): built from CpGs that change during development; and (3) interventional clock (int.DNAmAge): built from CpGs that change in response to aging related interventions such as caloric restriction, HFD, or dwarfing alleles[9,11,25]. These clocks were trained either in an independent mouse dataset that did not include the BXDs and were therefore unbiased to BXD characteristics (unbiased mouse clocks), or trained in a subset of the BXD CD mice and used to estimate age in the full BXD cohort (BXD-biased

Table 1. Epigenetic predictors and correlation with chronological age and entropy

Clock type	Training set[1]	DNAmAge name	Tissue	r with age (n=339)	r with entropy (n=339)
Standard	unbiased	DNAmAge	pan	0.89	0.50
Standard	unbiased	DNAmAge	liver	0.92	0.51
Developmental	unbiased	dev.DNAmAge	pan	0.87	0.46
Developmental	unbiased	dev.DNAmAge	liver	0.91	0.45
Interventional	unbiased	int.DNAmAge	pan	0.85	0.38
Interventional	unbiased	int.DNAmAge	liver	0.86	0.49
Standard	BXD	DNAmAge	pan	0.93	0.55
Standard	BXD	DNAmAge	liver	0.97	0.54
Developmental	BXD	dev.DNAmAge	pan	0.95	0.51
Developmental	BXD	dev.DNAmAge	liver	0.96	0.51
Interventional	BXD	int.DNAmAge	pan	0.89	0.43
Interventional	BXD	int.DNAmAge	liver	0.94	0.53
Universal	unbiased	univ.DNAmAge	pan	0.92	0.59
Lifespan	unbiased	Predicted-maxLS	pan	-0.07 (ns)	-0.13 (p=0.02)

[1] *Unbiased* denotes that the clocks were trained in a completely independent dataset.

clocks). In addition to the mouse clocks, we estimated DNAmAge using the universal mammalian clock (univ.DNAmAge)[15]. The clocks performed well in age estimation (**Table 1; Fig 1a**). The EAA derived from these clocks showed wide individual variation (**Fig 1b**), but the EAA values are uncorrelated with chronological age.

We used the universal maximum lifespan predictor[17] to estimate the potential maximum lifespan (predicted-maxLS) of mice. Predicted-maxLS was uncorrelated with chronological age (**Table 1**), and this is expected since the chronological age represents the time when the biospecimens were collected; not the time of natural demise. Instead, the predicted-maxLS showed an overall inverse correlation with EAA from the different clocks, and this suggests higher age-acceleration for mice with lower predicted-maxLS (**Data S2**).

Association with methylome entropy

The methylome-wide entropy provides a measure of randomness and information loss, and this increased with chronological age (**Fig 1c**)[7]. As direct correlates of chronological age, all the DNAmAge were positively correlated with entropy (**Table 1**).

We hypothesized that higher entropy levels will be associated with (a) higher EAA, and (b) lower predicted-maxLS. Indeed, the univ.EAA had a significant positive correlation with entropy that was significant regardless of diet (**Fig 1d**). However, the EAA from the unbiased mouse clocks showed only weak correlations with entropy (**Data S2**). Entropy had a modest negative correlation with predicted-maxLS primarily in the CD group (**Fig 1e**). Taken together, our results indicate that discordance in the methylome increases with age, and is higher with higher univ.EAA. Mice with shorter predicted-maxLS may also had slightly higher entropy.

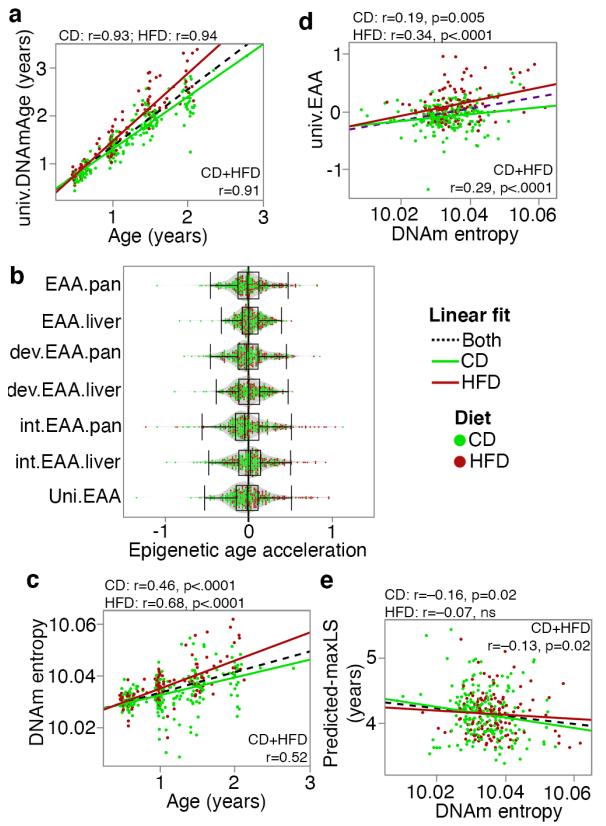

Fig 1. DNA methylation readouts and inter-correlations

(a) Correlation between predicted age (universal clock), and known chronological age. Mice on control diet depicted by green dots (CD; normal lab chow; n = 210); mice on high fat diet (HFD; n = 129) by red dots. **(b)** Violin plots of epigenetic age acceleration (EAA) derived from different DNAmAge clocks. **(c)** Shannon entropy, calculated from the full set of high quality CpGs, increases with age. **(d)** DNA methylation entropy has a direct correlation with EAA derived from the universal clock. **(e)** There is a slight inverse correlation between the entropy and DNA methylation based predicted maximum lifespan (predicted-maxLS).

How the epigenetic readouts relate to diet, body weight, and sex

Diet. EAA from most of the clocks, including the universal clock, were significantly higher in the HFD (**Table 2**). Entropy was also significantly higher in the HFD group. The maxLS did not differentiate between diets **(Table 2**).

Body weight. Body weight was first measured when mice were at an average age of 4.5 ± 2.7 months. We refer to this initial weight as baseline body weight (BW0). For mice on HFD, this

Table 2. Association with diet and weight, and heritability of the epigenetic readouts

Type	EAA	Diet	Mean (SD)	Diet (p)	r BW0 [a]	p BW0	r BWF [a]	p BWF	H^2	Strain r [b]
Unbiased DNAm clocks	EAA, pan	CD	-0.05 ± 0.21	<.0001	0.19	0.006	0.29	<.0001	0.49	0.54
		HFD	0.07 ± 0.21		0.21	0.01	0.42	<.0001	0.50	
	EAA, liver	CD	0 ± 0.17	ns	0.09	ns	0.20	0.003	0.40	0.73
		HFD	0.03 ± 0.14		0.22	0.01	0.49	<.0001	0.52	
	dev.EAA, pan	CD	-0.04 ± 0.23	0.004	0.09	ns	0.22	0.001	0.53	0.76
		HFD	0.03 ± 0.22		0.27	0.002	0.45	<.0001	0.61	
	dev.EAA, liver	CD	0 ± 0.2	ns	0.19	0.002	0.29	<.0001	0.46	0.78
		HFD	0 ± 0.16		0.29	0.0007	0.47	<.0001	0.60	
	int.EAA, pan	CD	-0.05 ± 0.25	0.0003	0.03	ns	0.21	0.002	0.27	0.66
		HFD	0.06 ± 0.33		0.22	0.01	0.46	<.0001	0.45	
	int.EAA, liver	CD	-0.04 ± 0.22	<.0001	0.05	ns	0.18	0.01	0.59	0.80
		HFD	0.11 ± 0.25		0.27	0.002	0.58	<.0001	0.54	
BXD biased DNAm clocks	EAA.BXD, pan	CD	-0.06 ± 0.15	<.0001	0.08	ns	0.17	0.01	0.26	0.22
		HFD	0.09 ± 0.19		0.17	0.05	0.37	<.0001	0.42	
	EAA.BXD, liver	CD	0 ± 0.11	0.01	-0.04	ns	0.06	ns	0.18	0.37
		HFD	0.03 ± 0.11		0.18	0.04	0.41	<.0001	0.34	
	dev.EAA.BXD, pan	CD	-0.03 ± 0.13	<.0001	-0.08	ns	0	ns	0.25	0.43
		HFD	0.05 ± 0.16		0.13	ns	0.40	<.0001	0.49	
	dev.EAA.BXD, liver	CD	-0.01 ± 0.13	0.002	0.07	ns	0.11	ns	0.26	0.45
		HFD	0.03 ± 0.12		0.21	0.02	0.47	<.0001	0.40	
	int.EAA.BXD, pan	CD	-0.05 ± 0.19	<.0001	0	ns	0.18	0.01	0.19	0.72
		HFD	0.07 ± 0.3		0.20	0.03	0.42	<.0001	0.41	
	int.EAA.BXD, liver	CD	-0.03 ± 0.16	<.0001	-0.04	ns	0.06	ns	0.39	0.78
		HFD	0.09 ± 0.16		0.23	0.01	0.60	<.0001	0.40	
Universal clock	univ.EAA	CD	-0.08± 0.22	<.0001	0	ns	0.11	ns	0.37	0.67
		HFD	0.13 ± 0.27		0.35	<.0001	0.50	<.0001	0.43	
Entropy	-	CD	10.034 ± 0.007	0.004	-0.15	0.03	-0.34	<.0001	0.39	0.20 (ns)
		HFD	10.036 ± 0.007		-0.11	0.21	0	ns	0.23	
Pred-maxLS	-	CD	4.14 ± 0.37	ns	0.03	ns	0.05	ns	0.66	0.89
		HFD	4.15 ± 0.32		-0.06	ns	-0.11	0.20	0.70	

[a] BW0 is body weight at about 4.5 months of age (n = 339; 210 CD and 129 HFD); BWF is final weight at tissue collection (1 HFD case missing data; n = 338; 210 CD and 128 HFD)

[b] Pearson correlation between strain means for n = 29 BXD genotypes kept on CD and HFD

was usually before introduction to the diet, with the exception of 48 cases that were first weighed 1 or 3 days after HFD (**Data S1**). In the CD group, only the unbiased EAA (pan-tissue) and dev.EAA (liver) showed significant positive correlations with BW0 (**Table 2**). In the HFD group, the positive correlation with BW0 was more robust and consistent across all the clocks, and this may have been due to the inclusion of the 48 cases that had been on HFD for 1 or 3 days. Taking only these 48 cases, we found that higher weight even after 1 day of HFD had an age-accelerating effect (**Data S2**). This was particularly strong for the unbiased interventional clocks (r = 0.45, p = 0.001 for int.EAA, pan-tissue; r = 0.58, p < 0.0001 for int.EAA, liver), and for the universal clock (**Fig 2a**). Second weight was measured 7.4 ± 5.2 weeks after BW0 (mean age 6.3 ± 2.8 months). We refer to this as BW1 and we estimated the weight change as deltaBW = BW1 – BW0. DeltaBW was a positive correlate of EAA on both diets, albeit more pronounce in the HFD group (**Fig 2b**; **Data S2**). The final body weight (BWF) was measured at the time of tissue harvest, and EAA from all the unbiased clocks were significant correlates of BWF on both diets **(Table 2**).

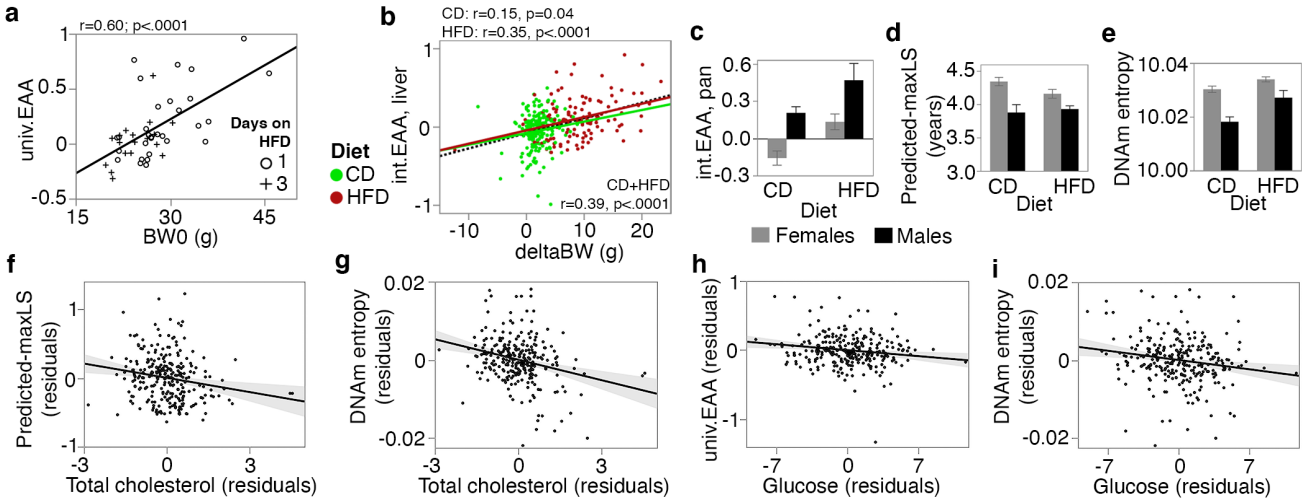

Fig 2. Correlates and modifiers of the epigenetic readouts

(a) For 48 mice, initial body weight (BW0) was measured 1 or 3 days after high fat diet (HFD), and these showed significant correlation between BW0 and epigenetic age acceleration (EAA shown for the universal clock). **(b)** Weight was first measured at mean age of 4.5 ± 2.7 months, and then at 6.3 ± 2.8 months (BW1). Weight gains during this interval (deltaBW = BW1 – BW0) is a direct correlate of EAA derived from the interventional clock in both normal chow (control diet or CD; n = 210) and HFD mice (n = 128). **(c)** For the BXD genotypes with samples from both males and females, males have higher age acceleration and this sex effect is highly significant for the pan-tissue interventional clock (int.EAA). Bars represent mean ± standard error; 40 females (26 CD, 14 HFD) and 18 males (10 CD, 8 HFD). Males had **(d)** lower predicted maximum-lifespan, and **(e)** lower average methylome entropy. **(f–i)** The residual plots display the direction of association between metabolic traits and DNAm readouts (n = 276 cases with metabolic data). After adjusting for chronological age, diet and body weight, serum cholesterol has inverse associations with **(f)** predicted maximum lifespan (p = 0.002), and **(g)** methylome entropy (p = 9.1E-06). Serum glucose level has inverse associations with **(h)** epigenetic age acceleration derived from the universal clock (p = 0.005), and **(i)** methylome entropy (p = 0.003).

Somewhat unexpected, entropy had an inverse correlation with body weight. This effect was primarily in the CD mice **(Table 2)**. We found no association between predicted-maxLS and the body weight traits (**Table 2**).

Sex effect. Four BXD genotypes (B6D2F1, D2B6F1, BXD102, B6) had cases from both males and females. We used these to test for sex effects. All the unbiased mouse clocks showed significant age acceleration in male mice, and this effect was particularly strong for the pan-tissue int.EAA (**Fig 2c; Data S2**). The predicted-maxLS was significantly lower in males (**Fig 2d**). Entropy on the other hand, was significantly higher in females (**Fig 2e**).

Association with metabolic traits

276 cases with DNAm data also had fasted serum glucose and total cholesterol[18,19], and we examined whether these metabolic traits are associated with the DNAm readouts. We applied regression analysis with age, diet and final body weight as covariates, and this showed significant effects of cholesterol on predicted-maxLS (p = 0.002), and entropy (p = 9E-06) (**Table S1**). To visualize how cholesterol levels associate with these, we plotted the residual values after the respective predictor and outcome variables were adjusted for age, diet, and BWF. The residual plot shows an inverse association between cholesterol and predicted-maxLS (**Fig 2f**). For entropy, similar to how it related with weight, higher cholesterol predicted lower entropy. Cholesterol had no significant association with univ.EAA **(Table S1)**.

Glucose had an unexpected inverse association with the univ.EAA that predicts lower age acceleration with higher glucose (p = 0.005) (**Fig 2h; Table S1**). Lower glucose also predicted higher entropy (p = 0.003) **(Fig 2i**). Glucose was not associated with predicted-maxLS **(Table S1)**.

Association with strain longevity

We next obtained longevity data from a parallel cohort of female BXD mice that were allowed to age on CD or HFD [18]. We evaluated whether the DNAm readouts were informative of strain-level lifespan. Since the strain lifespan was determined from female BXDs, we restricted this to only the female cases. For strains with natural death data from n ≥ 5, we computed the minimum (minLS), 25th quartile (25Q-LS), mean, median lifespan, 75th quartile (75Q-LS), and maximum lifespan (maxLS) (**Data S1**). Specifically, we postulated (a) an accelerated clock for strains with shorter lifespan (i.e., inverse correlation), (b) a direct correlation between predicted-maxLS and observed lifespan, and (c) higher entropy with shorter lifespan.

Overall, the EAA measures showed the expected inverse correlation trend with the lifespan summaries, and this was highly significant for the universal clock (**Table S2**; **Fig 3a**,**b**). For the mouse clocks, this effect was significant for the liver int.EAA (**Table S2**). When separated by diet, these correlations became weaker, but the negative trend remained consistent.

The DNAm entropy had an inverse correlation trend with strain lifespan (**Table S2**). This was nominally significant only for the strain maxLS when CD and HFD groups were combined (r = –0.13, p = 0.02) but became non-significant when separated by diet.

The predicted-maxLS showed a positive correlation trend with the lifespan summaries, and this was significant for the observed strain maxLS (**Fig 3d**). When separated by diet, the predicted-maxLS remained a significant correlate of strain maxLS only in the CD group.

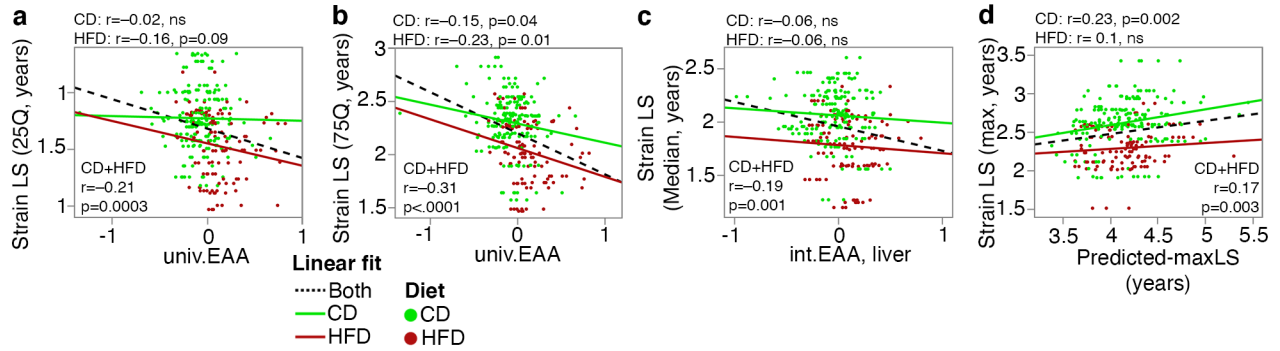

Fig 3. Predictors of strain longevity

BXD genotypes with shorter life expectancy tended to have a more accelerated universal clock (univ.EAA). This inverse relation is depicted for the **(a)** 25th and **(b)** 75th quartile age at natural death for female BXDs kept on either normal chow (CD) or high fat diet (HFD). **(c)** Age acceleration from the liver interventional unbiased mouse clock (int.EAA) also showed a similar inverse correlation with strain longevity, but effect was significant only when both diets were included (here illustrated with median lifespan). **(e)** The predicted maximum lifespan had a significant direct correlation with the observed strain maximum lifespan. Analysis in n = 302 female BXDs; 191 CD and 111 HFD.

Genetic analysis of epigenetic age acceleration and predicted-maxLS

The EAA traits had modest to high heritability, and averaged at 0.50 for the unbiased mouse clocks (**Table 2**). The predicted-maxLS had heritability of 0.66 on CD, and 0.70 on HFD. Another way to gauge level of genetic correlation is to compare between members of strains maintained on different diets. The EAA from the unbiased and universal clocks, and predicted-maxLS had high strain-level correlations between diets that indicates an effect of background genotype that is robust to dietary differences (**Table 2**). The genotype correlations were slightly lower for the BXD-biased clocks.

To uncover genetic loci, we applied QTL mapping using mixed linear modeling that corrects for the BXD kinship structure[31]. First, we performed the QTL mapping for each of the unbiased mouse and universal clocks, with adjustment for diet and body weight. EAA from the two interventional clocks had the strongest QTLs (**Data S3**). The pan-tissue int.EAA had a significant QTL on Chr11 (90–99 Mb) with the highest linkage at ~93 Mb (p = 3.5E-06; equivalent to a LOD score of 4.7) (**Fig 4a**). Taking a genotype marker at the peak interval (BXD variant ID DA0014408.4 at Chr11, 92.750 Mb)[20], we segregated the BXDs homozygous for either the D2 (*DD*) or the B6 (*BB*) alleles. The *DD* genotype had a significantly more accelerated int.EAA (**Fig 4a** inset). The liver int.EAA had the peak QTL on Chr19 (35–45 Mb) with the most significant linkage at markers between 38–42 Mb (p = 9E-07; LOD score of 5.2) (**Fig 4b**). We selected a marker at the peak interval (rs48062674 at Chr19, 38.650 Mb), and the *BB* genotype had significantly higher int.EAA compared to *DD* (**Fig 4b** inset). The QTL map for the univ.EAA did not reach genome-wide significance (**Fig 4c**). However, there were nominally significant peaks at the Chr19 (p = 0.0004), and Chr11 (p = 0.004) intervals.

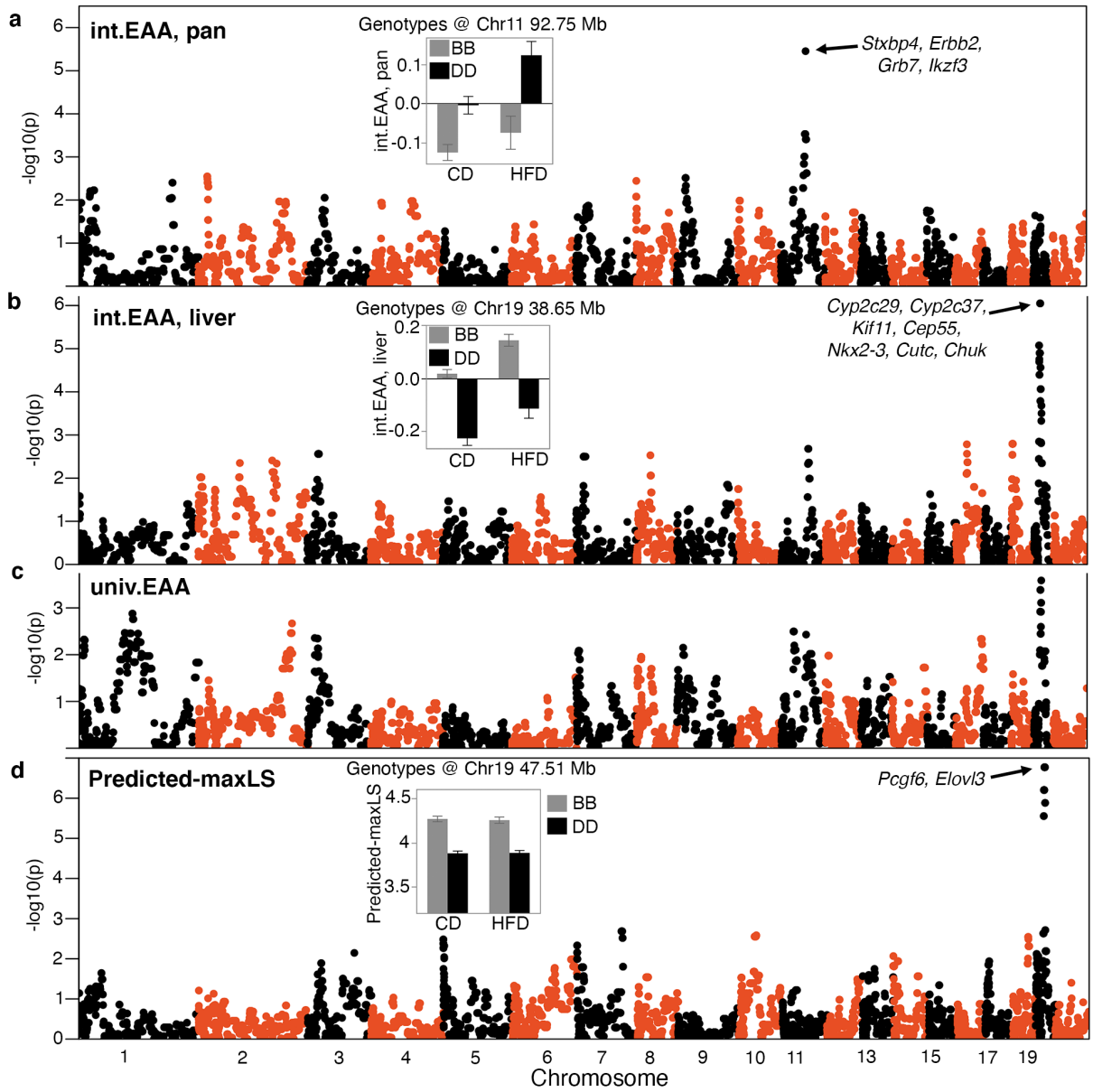

Fig 4. Genetic linkage analysis

The Manhattan plots represent the location of genotyped markers (x-axis), and linkage – $\log_{10}p$ (y-axis). **(a)** The peak quantitative trait locus (QTL) for age acceleration from the pan-tissue interventional clock (int.EAA) is on chromosome (Chr) 11 at ~93 Mb. The inset shows the mean (± standard error) trait values for BXDs the are homozygous for the C57BL/6J allele (*BB*; grey) versus BXDs homozygous for the DBA/2J allele (*DD*; black). **(b)** The liver-specific int.EAA has a peak QTL on Chr19 (~38 Mb). Trait means by genotype at this locus are shown in inset. **(c)** The linkage statistics are weaker for the EAA derived from the universal clock (univ.EAA). However, there are consistent nominally significant peaks on the Chr11 and Chr19 loci. **(d)** The DNA methylation based predicted maximum lifespan also maps to Chr19, but the peak markers are at ~47.5 Mb.

We next performed QTL mapping for DNAm entropy with adjustment for major covariates (diet,

222 chronological age, and body weight). No locus reached genome-wide significance (**DataS3**).
223 There were modest QTLs on Chrs11 and 19. However, the Chr11 region is slightly distal to the
224 markers linked to the EAA traits (minimum p = 0.009 at Chr11, ~103.7 Mb). The Chr19 locus
225 somewhat overlapped the QTL for EAA, but the peak marker (minimum p = 0.0009) is slightly
226 distal at ~48 Mb (**Data S3**).

227 The predicted-maxLS had a significant QTL on Chr19 (**Fig 4d; Data S3**) with the peak markers
228 between 44–48 Mb (p = 2E-07; LOD score of 5.9). This overlaps the EAA QTL, but the peak
229 markers are also distal (rs30567369 at 47.510 Mb). At this locus, mice with the *BB* genotype
230 had significantly higher predicted-maxLS (**Fig 4d** inset).

231 Consensus QTLs for epigenetic age acceleration

232 To identify regulatory loci that are consistent across the different EAA measures, we applied a
233 multi-trait analysis and derived the linkage meta-p-value for the unbiased mouse and universal
234 EAA traits[32]. The peaks on Chrs 11 and 19 attained the highest consensus p-values (**Fig S1a;**
235 **Data S3**). Additional consensus peaks (at $-\log_{10}$meta-p > 6) were observed on Chrs 1 (~152 Mb),
236 and 3 (~54 Mb).

237 We focus on the Chrs 11 and 19 QTLs and refer to these as *EAA QTL on Chr 11* (*Eaaq11*), and
238 *EAA QTL on Chr 19* (*Eaaq19*). *Eaaq11* extends from 90–99 Mb. For *Eaaq19*, we delineated a
239 broader interval from 35–48 Mb that also encompasses the peak markers for the predicted-
240 maxLS, albeit these may be separate loci related to EAA (~39 Mb of *Eaaq19*), and predicted-
241 maxLS (~47 Mb of *Eaaq19*).

242 We performed marker-specific linkage analyses for each of the unbiased mouse and universal
243 clocks using a regression model that adjusted for diet. With the exception of the liver int.EAA,
244 all the EAA traits had nominal to highly significant associations with the representative *Eaaq11*
245 marker (DA0014408.4), and the *DD* genotype had higher age acceleration (**Table 3**). Mean plots
246 by genotype and diet shows that this effect was primarily in the CD mice (**Fig S1b**). The effect of
247 this locus appeared to be higher for the pan-tissue clocks compared to the corresponding liver-
248 specific clocks. This marker in *Eaaq11* was not associated with either entropy or predicted-
249 maxLS.

250 For proximal *Eaaq19*, the representative marker (rs48062674) was associated with all the EAA
251 traits and the *BB* mice had higher age acceleration on both diets (**Fig S1c**). This marker was not
252 associated with entropy, and had only a weak effect on predicted-maxLS (**Table 3**). When we
253 performed the same analysis with the marker on distal *Eaaq19* (rs30567369), the association
254 with EAA became weaker, and the association with predicted-maxLS became much stronger
255 (**Table 3**). This suggests that the proximal part of *Eaaq19* is related to EAA while the distal part
256 is related to predicted-maxLS.

257 We also tested if these peak markers were associated with the recorded lifespan phenotype
258 and we found no significant association with the observed lifespan of the BXDs.

259 Association of EAA QTLs with body weight trajectory

Table 3: Marker specific linkage analyses for epigenetic age acceleration, predicted maximum lifespan, and body weight trajectory

Predictor	Outcome	Estimate	Std Error	t Ratio	p
Eaaq11 DA0014408.4[DD] Chr11, 92.750 Mb (133 *BB* cases, and 173 *DD* cases)	EAA, pan	0.096	0.023	4.184	3.8E-05
	EAA, liver	0.067	0.017	3.880	0.0001
	dev.EAA, pan	0.077	0.025	3.041	0.003
	dev.EAA, liver	0.037	0.020	1.878	0.06
	int.EAA, pan	0.153	0.029	5.278	2.5E-07
	int.EAA, liver	-0.033	0.025	-1.284	0.20
	univ.EAA	0.101	0.025	4.057	6.3E-05
Eaaq19 rs48062674[DD] Chr19, 38.650 Mb (238 *BB* cases, and 67 *DD* cases)	EAA, pan	-0.083	0.028	-2.954	0.003
	EAA, liver	-0.137	0.020	-6.972	2.0E-11
	dev.EAA, pan	-0.206	0.029	-7.218	4.3E-12
	dev.EAA, liver	-0.124	0.023	-5.461	9.9E-08
	int.EAA, pan	-0.143	0.035	-4.028	7.1E-05
	int.EAA, liver	-0.250	0.027	-9.238	4.6E-18
	univ.EAA	-0.145	0.029	-4.932	1.3E-06
	Pred-maxLS	-0.100	0.048	-2.086	0.04
Distal Eaaq19 rs30567369[DD] Chr19, 47.510 Mb (198 *BB* cases, and 106 *DD* cases)	int.EAA, liver	-0.079	0.026	-2.995	0.003
	univ.EAA	-0.053	0.026	-2.012	0.05
	Pred-maxLS	-0.383	0.036	-10.781	3.9E-23
Mixed model for longitudinal change in body weight					
Predictor	**Outcome**	**Estimate**	**Std Error**	**t Ratio**	**p**
Eaaq11 DA0014408.4[DD] Number of observations = 6885; number of individuals = 2112	Body weight	0.619	0.345	1.794	0.07
Eaaq19 rs48062674[DD] Number of observations = 6132; number of individuals = 1852	Body weight	-1.847	0.374	-4.945	7.6E-07
Distal Eaaq19 rs30567369[DD] Number of observations = 6059; number of individuals = 1802	Body weight	-1.619	0.363	-4.458	8.3-06

Since body weight gains was an accelerator of the clocks, we examined whether the selected markers in *Eaaq11* and *Eaaq19* were also related to body weight change. We retrieved longitudinal weight data from a larger cohort of the aging BXD mice that were weighed at

263 regular intervals. After excluding
264 heterozygotes, we tested the effect of
265 genotype. Concordant with the higher
266 EAA for the *DD* genotype at *Eaaq11* in the
267 CD group, the *DD* genotype in the CD
268 group also had slightly higher mean
269 weight at older adulthood (12 and 18
270 months; **Fig 5a**). However, this marker
271 had no significant association with body
272 weight when tested using a mixed effects
273 model (p = 0.07; **Table 3**). In proximal
274 *Eaaq19*, it was the *BB* genotype that
275 exhibited consistently accelerated clock
276 on both diets, and the *BB* genotype also
277 had higher average body weight by 6
278 months of age (**Fig 5b**), and this locus had
279 a significant influence on the body weight
280 trajectory (p = 7.6E-07; **Table 3**). The
281 nearby marker on distal *Eaaq19* also
282 showed a similar pattern of association
283 with body weight (**Table 3**).

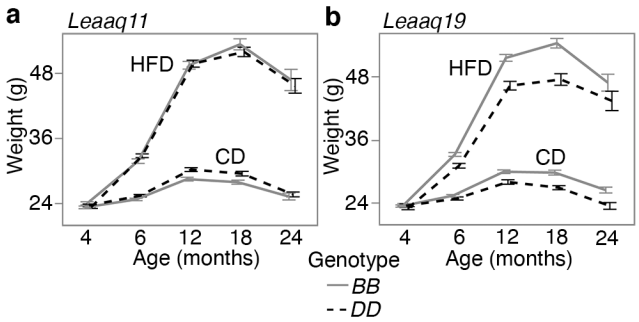

Fig 5. Body weight trajectory by diet and genotype
Body weight was measured at regular age intervals (x-axis) from **(a)** 2112 BXD mice that were homozygous at the *Leaaq11* marker (DA0014408.4; 842 *BB*, 1279 *DD*), and **(b)** 1852 BXD mice that were homozygous at the proximal *Leaaq19* marker (rs48062674; 1252 *BB*, 600 *DD*). Mice were maintained on either control diet (CD) or high fat diet (HFD). The graphs show the segregation of body weight over time by diet and genotype. Mean ± standard error; heterozygotes were excluded.

284 Candidate genes for epigenetic age 285 acceleration

286 There are several positional candidate genes in *Eaaq11* and *Eaaq19*. To narrow the list, we
287 applied two selection criteria: genes that (1) contain missense and/or stop variants, and/or (2)
288 contain non-coding variants and regulated by a cis-acting expression QTL (eQTL). For the eQTL
289 analysis, we utilized an existing liver transcriptome data from the same aging cohort[19]. We
290 identified 24 positional candidates in *Eaaq11* that includes *Stxbp4*, *Erbb2* (*Her-2* oncogenic
291 gene), and *Grb7* (growth factor receptor binding) (**Data S4**). *Eaaq19* has 81 such candidates that
292 includes a cluster of cytochrome P450 genes, and *Chuk* (inhibitor of NF-kB) in the proximal
293 region, and *Pcgf6* (epigenetic regulator) and *Elovl3* (lipid metabolic gene) in the distal region
294 (**Data S4**).

295 For further prioritization, we converted the mouse QTL regions to the corresponding syntenic
296 regions in the human genome, and retrieved GWAS annotations for these regions[33]. We
297 specifically searched for the traits: epigenetic aging, longevity, age of
298 menarche/menopause/puberty, Alzheimer's disease, and age-related cognitive decline and
299 dementia. This highlighted 5 genes in *Eaaq11*, and 3 genes in *Eaaq19* (**Table S4**). We also
300 identified a GWAS study that found associations between variants near *Myof-Cyp26a1* and
301 human longevity[30], and a meta-GWAS that found gene-level associations between *Nkx2–3* and
302 *Cutc*, and epigenetic aging[28] (**Table S4**).

303 Gene expression correlates of EAA and predicted max-LS

304 Liver RNA-seq data was available for 153 of the BXD cases that had DNAm data (94 CD, and 59
305 HFD)[19]. We used this set to perform transcriptome-wide correlation analysis for the univ.EAA.
306 To gain insights into gene functions, we selected the top 2000 transcriptome correlates (|r| ≥
307 0.37, p ≤ 2.8E-06; **Data S5**) for functional enrichment analysis. These top correlates represented
308 transcript variants from 1052 unique genes and included a few positional candidates (e.g., *Ikzf3*,
309 *Kif11*, *Cep55*, *Cyp2c29*, *Cyp2c37*). Only 62 transcripts from 36 unique genes were negatively
310 correlated with univ.EAA, and this set was significantly enriched (Bonferroni correct p < 0.05) in
311 oxidation-reduction, and metabolic pathways (**Data S6**; **Fig 6a**). These functional categories
312 included the cytochrome genes, *Cyp2c29* and *Cyp2c37*, located in *Eaaq19*. This set was also
313 highly liver specific. The positive correlates were enriched in a variety of gene functions, and

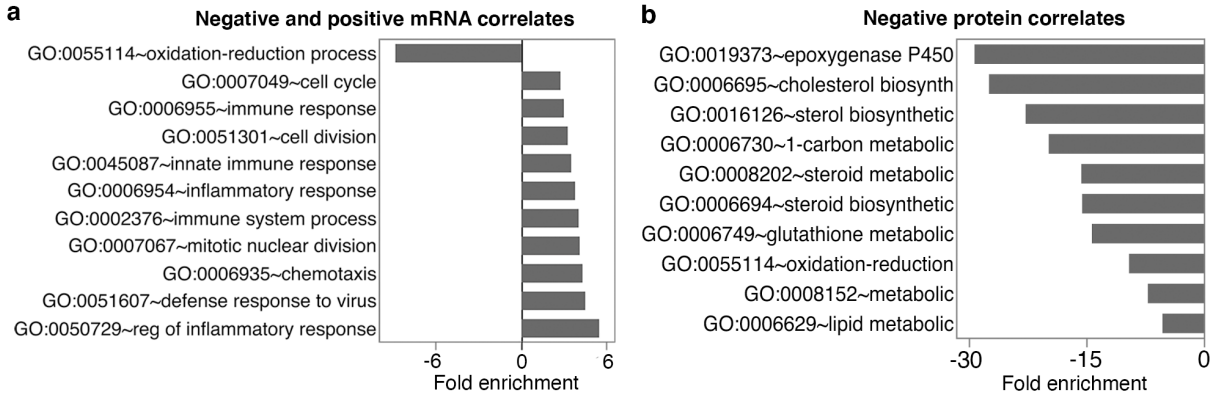

Fig 6. Gene expression correlates of the universal clock
(a) Graph displays the enriched gene ontologies (GO) for the top 2000 transcriptome correlates of epigenetic age acceleration (univ.EAA). The y-axis shows the fold enrichment; positive values are for the positive correlates, and negative values are for the negative correlates of univ.EAA. The smaller set of negative mRNA correlates is enriched in oxidation-reduction process. For positive mRNA correlates, the top 10 enriched GOs highlight immune response, cell cycle, and mitosis. **(b)** The top 10 negative proteome correlates of univ.EAA is also enriched in oxidation-reduction and related metabolic pathways, and these are populated by several cytochrome P450 genes.

314 was not a liver-specific gene set (**Data S6**). Taking the top 10 GO categories, we can broadly
315 discern two functional domains: immune and inflammatory response, and mitosis and cell cycle
316 (**Fig 6a**). To verify that these associations are robust to the effect of diet, we repeated the
317 correlation and enrichment analysis in the CD group only (n = 94). Again, taking the top 2000
318 correlates (|r| ≤ 0.30; p ≤ 0.003), we found the same enrichment profile for the positive and
319 negative correlates (**Data S6**).

320 Next, we performed the correlational analysis using liver proteomic data that was available for
321 164 of the BXDs. The proteome data quantifies over 32000 protein variants from only 3940
322 unique genes[19]. We took the top 2000 protein correlates of univ.EAA (|r| ≥ 0.27, p ≤ 6.0E-04)
323 (**Data S7**). This represented protein levels from 563 unique genes. 1139 protein variants (215
324 genes) had negative correlations, and similar to the mRNA correlates, there was enrichment in
325 oxidation-reduction and metabolic processes. This set was also enriched in liver genes, and

326 included pathways related to lipid and steroid metabolism, epoxygenase p450 pathway, and
327 xenobiotics (**Fig 6b**; **Data S8**). These categories were populated by the cytochrome genes
328 including candidates in *Eaaq19* (e.g., *Cyp2c29*, *Cyp2c37*). The positive proteome correlates
329 showed a different functional profile than the transcriptomic set. These were enriched in genes
330 related to transport (includes apolipoprotein such as APOE), cell adhesion, protein translation,
331 protein folding, and metabolic pathways related to glycolysis and gluconeogenesis (**Data S8**).

332 We performed a similar transcriptome and proteome analysis for the predicted-maxLS. For
333 mRNA, both the negative and positive correlates were enriched in metabolic pathways
334 including glucose and lipid metabolism (**Data S9, S10**). Similarly, the positive and negative
335 protein correlates of predicted-maxLS converged on oxidation-reduction processes (included
336 cytochrome genes located in proximal *Eaaq19*) and metabolic pathways (**Data S11, S12**).

337 Discussion

338 The goal of this study was to examine the aging methylome, its correlates and modifiers, and
339 potential genetic drivers. HFD had a strong age-accelerating effect that concurs with the
340 association between EAA and obesity in humans[25,34,35]. Age-acceleration due to diet manifested
341 within the first 1 to 3 days of transitioning from normal lab chow to HFD. Even among the CD
342 mice, higher weight gain at a younger age was associated with an accelerated clock.

343 Somewhat surprising was how entropy related to the metabolic traits. Epigenetic entropy
344 increases with age, and is likely an indicator of the level of stochastic noise that increases with
345 time[7,36]. In biological systems, entropy is kept at bay by the uptake of energy, and investment in
346 maintenance and repair[37]. As HFD increased entropy (possibly due to higher cellular
347 heterogeneity and adiposity of liver tissue), we expected entropy to be higher with higher body
348 weight. But instead, entropy had an inverse correlation with weight, an effect that was
349 primarily in the CD mice. Higher levels of serum glucose and total cholesterol were also
350 associated with lower entropy. The reason for this is unclear, and we can only speculate that
351 the enhanced energy consumption in mice that had higher metabolic substrates may have kept
352 the methylome in a more ordered state. Despite this, mice with higher entropy also tended to
353 have higher EAA. Entropy had a modest negative correlation with not only the DNAm based
354 predicted-maxLS, but also with the known strain-level maxLS. The predicted-maxLS on the
355 other hand, showed no direct association with diet or body weight, but higher total cholesterol
356 and EAA predicted shorter predicted-maxLS.

357 For the BXDs, life expectancy is highly dependent on the background genotype[18,22,24]. Similarly,
358 the universal and interventional clocks were more accelerated in mice belonging to strains with
359 shorter lifespan, and the predicted-maxLS also concurred with the observed strain maxLS. We
360 note that the predicted-maxLS overestimated the strain max-LS by 0.7 to 3 years (median error
361 of +1.6 years). Nonetheless, the correlation between individual-level predicted-, and strain-level
362 observed maxLS is remarkable considering that both the universal clock and max-LS predictor
363 are pan-mammalian, and species- and tissue-agnostic[17,38]. Our results suggest that these
364 universal epigenetic predictors of biological aging, and lifespan are informative of the subtle
365 and normative lifespan variation in a family of inbred mice. The analysis between the epigenetic
366 readouts and lifespan was also an indirect comparison. Unlike the comparison with body weight

367 and metabolic traits, which were traits measured from the same individual, the lifespan data
368 are strain characteristics computed from a parallel cohort of mice that were allowed to survive
369 till natural mortality. Nonetheless, this indirect comparison demonstrates that these epigenetic
370 predictors capture genotype-dependent effects.

371 We tested different versions of the mouse DNAmAge clocks, and these appeared to capture
372 slightly different aspects of epigenetic aging. For instance, the interventional clocks were
373 sensitive to diet and early weight change, but not related to BW0 in the CD mice. Instead, BW0
374 had a significant accelerating effect on the liver specific developmental clock (dev.EAA).

375 Our goal was to take these different clocks and identify regulatory loci that were the most
376 stable and robust to the slight algorithmic differences in building the clocks. A notable
377 candidate in *Eaaq11* is Syntaxin binding protein 4 (*Stxbp4*, aka, *Synip*), located at 90.5 Mb.
378 *Stxbp4* is a high-priority candidate due to the concordant evidence from human genetic studies.
379 The conserved gene in humans is a replicated GWAS hit for the intrinsic rate of epigenetic
380 aging[26-28]. In the BXDs, *Stxbp4* contains several non-coding variants, and a missense mutation
381 (rs3668623), and the expression of *Stxbp4* in liver is modulated by a *cis*-eQTL. *Stxbp4* plays a
382 key role in insulin signaling[39], and has oncogenic activity and implicated in different cancers[40,41].
383 Furthermore, GWAS have also associated *STXBP4* with age of menarche[42,43]. *Eaaq11*
384 corresponds to the 17q12-21 region in humans, and the location of additional oncogenic genes,
385 e.g., *ERBB2/HER2*, *GRB7*, and *BRCA1*[44]. The mouse *Brca1* gene is a little distal to the peak QTL
386 region and is not considered a candidate here, although it does segregate for two missense
387 variants in the BXDs. *Erbb2* and *Grb7* are in the QTL region, and *Erbb2* contains a missense
388 variant (rs29390172), and *Grb7* is modulated by a *cis*-eQTL. *Nr1d1* is another candidate in
389 *Eaaq11*, and the co-activation of *Erbb1*, *Grb7*, and *Nr1d1* has been linked to breast and other
390 cancers[45,46].

391 *Eaaq19* was consistently associated with EAA from all the clocks we evaluated, and also with
392 body weight gains, irrespective of diet. The predicted-maxLS also maps to this region, and
393 DNAm entropy may also have a weak association with markers at this interval. The EAA traits
394 have peak markers in the proximal part of *Eaaq19* (around the cytochrome cluster), and the
395 predicted-maxLS peaks in the distal portion (over candidates like *Elovl3*, *Pcgf3*). Two candidates
396 in *Eaaq19* have been implicated in epigenetic aging in humans based on gene-level meta-
397 GWAS: NK homeobox 3 (*Nkx2-3*, a developmental gene), and CutC copper transporter (*Cutc*)[28].
398 *Eaaq19* is also the location of the *Cyp26a1-Myof* genes, and the human syntenic region is
399 associated with longevity, metabolic traits, and lipid profiles [30,47,48]. Another noteworthy
400 candidate in *Eaaq19* is *Chuk*, a regulator of mTORC2, that has been associated with age at
401 menopause[42,49]. Clearly, *Eaaq19* presents a complex and intriguing QTL related to the different
402 DNAm readouts, and potentially metabolic traits. Both *Eaaq19* and *Eaaq11* exemplify the major
403 challenge that follows when a genetic mapping approach leads to gene- and variant-dense
404 regions [50,51]. Both loci have several biologically relevant genes, and identifying the causal gene
405 (or genes) will require a more fine-scaled functional genomic dissection.

406 The gene expression analyses highlighted metabolic pathways related to lipids, glucose, and
407 proteins for both the univ.EAA and predicted-maxLS. Other enriched pathways were mitosis
408 and cell division, and immune processes, but this was specific to the positive transcriptomic

409 correlates. The more compelling evidence is for the cytochrome P450 genes, which are both
410 positional candidates, as well as expression correlates at the transcriptomic and proteomic
411 levels. These genes have high expression in liver, and have major downstream impact on
412 metabolism[52-54]. One caveat is that these CYP genes are part of a gene cluster in *Eaaq19* that
413 includes transcripts with *cis*-eQTLs (e.g., *Cyp2c66*, *Cyp2c39*, *Cyp2c68*), and the tight clustering of
414 the genes, and proximity of trait QTL and eQTLs may result in tight co-expression due to linkage
415 disequilibrium [55]. Nonetheless, the cytochrome genes in *Eaaq19* are strong candidate
416 modulators of EAA that calls for further investigation.

417 Aside from *Eaaq11* and *Eaaq19*, loci with evidence of consensus QTLs were also detected on
418 Chrs 1 and 3. We do not delve into these in the present work, but the Chr3 interval is near
419 genes associated with human epigenetic aging (*Ift80*, *Trim59*, *Kpna4*)[26,28]. However, this QTL is
420 dispersed across a large interval, and the peak markers do not exactly overlap these human EAA
421 GWAS hits. While we have focused on *Eaaq11* and *Eaaq19*, these other loci also present
422 potentially important regions for EAA.

423 In summary, we have identified two main QTLs—*Eaaq11* and *Eaaq19*—that contribute to
424 variation in two DNAm readouts: EAA, and predicted-maxLS. *Eaaq11* contains several genes
425 with oncogenic properties (e.g., *Stxbp4*, *Erbb2*), while *Eaaq19* contains a dense cluster of
426 metabolic genes (e.g., *Elovl3*, *Chuk,* the cytochrome genes). We demonstrate that metabolic
427 profile and body weight are closely related to epigenetic aging. The convergence of evidence
428 from genetic and gene expression analyses suggests that genes involved in metabolism and
429 energy balance may modulate the age-dependent restructuring of the methylome, and this
430 may in turn, have an impact on the epigenetic predictors of aging and lifespan.

431 Materials and Methods

432 Biospecimen collection and processing

433 Samples for this study were selected from a larger colony of BXD mice that were housed in a
434 specific pathogen-free (SPF) facility at the University of Tennessee Health Science Center
435 (UTHSC). All animal procedures were in accordance with a protocol approved by the
436 Institutional Animal Care and Use Committee (IACUC) at the UTHSC. Detailed description of
437 housing conditions and diet can be found in [18,19]. Mice were given *ad libitum* access to water,
438 and either standard laboratory chow (Harlan Teklad; 2018, 18.6% protein, 6.2% fat, 75.2%
439 carbohydrates), or high-fat chow (Harlan Teklad 06414; 18.4% protein, 60.3% fat, 21.3%
440 carbohydrate). Animals were first weighed within the first few days of assignment to either
441 diets, and this was mostly but not always prior to introduction to HFD. Following this, animals
442 were weighed periodically, and a final time (BWF) when animals were humanely euthanized
443 (anesthetized with avertin at 0.02 ml per g of weight, followed by perfusion with phosphate-
444 buffered saline) at specific ages for tissue collection. The present work utilizes the biobanked
445 liver specimens that were pulverized and stored in -80 °C, and overlaps samples described in [19].
446 DNA was extracted using the DNeasy Blood & Tissue Kit from Qiagen. Nucleic acid purity was
447 inspected with a NanoDrop spectrophotometer, and quantified using a Qubit fluorometer
448 dsDNA BR Assay.

449 Methylation array, quality check, and entropy calculation

450 DNA samples from ~350 BXD mice were profiled on the Illumina HorvathHumanMethylChip40
451 array. Details of this array are described here[15].The array contains probes that target ~36K
452 highly conserved CpGs in mammals. Over 33K probes map to homologous regions in the mouse
453 genome, and data from these were normalized using the SeSame method [56]. Unsupervised
454 hierarchical clustering was performed to identify outliers and failed arrays, and these were
455 excluded. We also performed strain verification as an additional quality check. While majority
456 of the probes were free of DNA sequence variants, we found 45 probes that overlapped
457 variants in the BXD family. We leveraged these as proxies for genotypes, and performed a
458 principal component analysis. The top principal component (PC1 and PC2) segregated the
459 samples by strain identity, and samples that did not cluster with the reported strains were
460 removed. After excluding outliers, failed arrays, and samples that failed strain verification, the
461 final liver DNAm data consisted of 339 samples.

462 For entropy calculation, we used 27966 probes that have been validated for the mouse genome
463 using calibration data generated from synthetic mouse DNA[57]. Shannon entropy was calculated
464 for each sample using the R package, "entropy" (v1.2.1) with method = "ML": maximum
465 likelihood[58].

466 Clock estimation and maximum lifespan predictor

467 The development of the universal pan-tissue epigenetic clocks of age, and the universal
468 maximum lifespan predictor are described in Lu et al[38], and Li et al.[17], respectively. For the
469 present work, we utilized the universal clock that predicts relative age, defined as individual age
470 relative to the maximum lifespan of its species, followed by inverse transformation to estimate
471 DNAmAge[38]. The mouse specific clock were built using subsets of CpGs, and these will be
472 described in a companion paper. Age acceleration (EAA) measures were defined as the
473 residuals from regression of DNAm age on chronological age. By definition, EAA measures are
474 independent of age.

475 Statistics

476 Statistical analyses between the epigenetic predictors and continuous variables (body weight,
477 strain lifespan) were based on Pearson correlations, and t-test was used to evaluate the effect
478 of categorical predictors (sex, diet).

479 Two metabolic traits were downloaded from the bioinformatics platform GeneNetwork 2 (GN2)
480 [59]: (1) fasted serum glucose, and (2) fasted serum total cholesterol (more information on how
481 to retrieve these data directly from GN2 are provided in **Data S13**). Association with metabolic
482 traits was examined using multivariable linear regression (the R equations are provided in **Table**
483 **S1**). For visualization, residuals for both the predictor and outcome variables were extracted
484 after regressing on age, diet, and BWF using the R code: residuals(lm(~ age + diet + BWF)).

485 Longevity data (defined as age at natural death) was also downloaded from GN2 (**Data S13**)[18].
486 Males were excluded and strain-by-diet lifespan summary statistics were derived. Only strain-
487 by-diet groups with 5 or more observations were included in the correlational analyses with the
488 epigenetic predictors.

489 Genetic analyses

490 The broad sense heritability within diet was estimated as the fraction of variability that was
491 explained by background genotype[20,60,61]. For this, we applied a simple anova: aov(EAA ~
492 strain), and heritability was computed as $H^2 = SSq_{strain}/(SSq_{strain} + SSq_{residual})$, where SSq_{strain} is the
493 strain sum of squares, and $SSq_{residual}$ is the residual sum of squares.

494 All QTL mapping was done on the GN2 platform, and these traits can be accessed from this
495 website[59] (trait accession IDs provided in **Data S13**). In the GN2 home page, the present set of
496 BXD mice belongs to the **Group: BXD NIA Longevity Study**, and GN2 provides a direct interface
497 to the genotype data. All QTL mapping was done for genotypes with minor allele frequency ≥
498 0.05 using the genome-wide efficient mixed model association (GEMMA) algorithm[31], which
499 corrects for the BXD kinship matrix. For the EAA traits, diet, weight at 6 months, and final
500 weight were fitted as cofactor. Chronological age had not correlation with EAA and this was not
501 included as a cofactor (including age does not change the results). Genome-wide linkage
502 statistics were downloaded for the full set of markers that were available from GN2 (3720
503 markers as of early 2021). For the combined p-values, QTL mapping was done separately using
504 GEMMA for each EAA derived from all the unbiased mouse and universal clocks. Fisher's p-
505 value combination was then applied to get the meta-p-value[32]. We used this method to simply
506 highlight loci that had consistent linkage across the different EAA measures. QTL mapping for
507 entropy, major covariates—age, diet, BW1, and BWF—were included as co-factors. QTL
508 mapping for predicted-maxLS was done without co-factors as age, weight, and diet were not
509 significant covariates (including these do not change the results).

510 For marker specific linkage, we selected SNPs located at the peak QTL regions (DA0014408,
511 rs48062674, rs30567369), and grouped the BXDs by their genotypes (F1 hybrids and other
512 heterozygotes were excluded from this), and marker specific linkage was tested using ANOVA.
513 rs48062674 and rs30567369 are reference variants that is already catalogued in dbSNP[62], and is
514 used as a marker in the QTL mapping. DA0014408.4 is an updated variant at a recombinant
515 region in the Chr11 interval and within the peak QTL interval[20]. Genotypes at these markers for
516 individual BXD samples are in **Data S1**.

517 For marker specific QTL analysis for EAA, we performed linear regression using the data in **Data**
518 **S1**. Heterozygotes at the respective markers were excluded, and we applied the following
519 regression model for each of the unbiased mouse and universal EAA separately: lm(EAA ~
520 genotype + diet). To test the effect on body weight change, body weight data measured at
521 approximately 4 (baseline), 6, 12, 18, and 24 months were downloaded from GN2 (**Data S13**).
522 Detailed description of these weight data are in Roy et al[18]. We then applied a mixed effects
523 regression model using the lme4 R package[63]: lmer(weight ~ age + diet + genotype + (1|ID)),
524 where ID is the identifier for individual mouse.

525 Bioinformatic tools for candidate gene selection

526 Sequence variation between B6 and D2 in the QTL intervals (Chr11:90–99 Mb, and Chr19:35–48
527 Mb) were retrieved from the Wellcome Sanger Institute Mouse Genomes Project database
528 (release 1505 for GRCm38/mm10)[64-66]. Positional candidates were required to contain at least
529 one coding variant (missense and/or nonsense variants), or have non-coding variants with
530 evidence of *cis*-regulation in liver tissue of the BXDs. *Cis*-eQTLs for the candidate genes were
531 obtained from the liver RNA-seq data described in[19]. An interface to search and analyze this

532 transcriptome data is available from GN2, and is catalogued under *Group: BXD NIA Longevity*
533 *Study*; *Type: Liver mRNA*; and *Dataset: UTHSC BXD Liver RNA-seq (Oct 19) TMP Log2*. This data
534 was also used for the transcriptome-wide correlations analysis for univ.EAA in the 153 cases
535 that had both DNAm and RNA-seq data. We considered the top 2000 highest correlated
536 transcripts, and the list of transcripts were collapsed to a non-redundant list of gene symbols,
537 and this was uploaded to the DAVID Bioinformatics Database (version 6.8) for GO enrichment
538 analysis[67,68]. Similarly, proteome correlational analysis was carried out using the data: *Group:*
539 *BXD NIA Longevity Study*; *Type: Liver Proteome*; and *Dataset: EPFL/ETHZ BXD Liver Proteome*
540 *CD-HFD (Nov19)* [19].

541 For human GWAS annotations, we navigated to the corresponding syntenic regions on the
542 human genome by using the coordinate conversion tool in the UCSC Genome Browser. The
543 Chr11 90–95 Mb interval on the mouse reference genome (GRCm38/mm10) corresponds to
544 human Chr17:50.14–55.75 Mb (GRCh38/hg38) (40.7% of bases; 100% span). The Chr11 95–99
545 Mb interval in the mouse corresponds to human Chr17:47.49–50.14 Mb (29.3% of bases, 57.9%
546 span), and Chr17:38.19–40.39 Mb (20.7% of bases, 44.1% span). Likewise, for the Chr19 QTL,
547 the mm10 35–40 Mb corresponds to hg38 Chr10:89.80–95.06 Mb (32.2% of bases, 89.2% span),
548 40–45 Mb corresponds to hg38 Chr10:95.23–100.98 Mb (46.6% of bases, 95.6% span), and 45–
549 48 Mb corresponds to hg38 Chr10:100.98–104.41 Mb (46.5% of bases, 100% span). We then
550 downloaded the GWAS data for these regions from the NHGRI-EBI GWAS catalogue[33], and
551 retained the GWAS hits that were related to aging.

552 Data availability

553 The full microarray data will be released via NCBI's Gene Expression Omnibus upon official
554 publication. Genome annotations of the CpGs can be found on Github
555 https://github.com/shorvath/MammalianMethylationConsortium. Individual level BXD data are
556 available on www.genenetwork.org on FAIR+ compliant format; data identifiers, and way to
557 retrieve data are described in **Data S13**.

558 **Acknowledgement.** We thank the entire UTHSC BXD Aging Colony team, particularly
559 Casey J Chapman, Melinda S McCarty, Jesse Ingles, and everyone else who contributed to the
560 tissue harvest. We thank Evan G Williams for making the gene expression data readily available,
561 and to David Ashbrook for providing the BXD genotypes. We thank the GeneNetwork team,
562 especially Zach Sloan and Arthur Centeno, who have been extremely prompt and effective at
563 assisting with the GeneNetwork interface.

564 **Author contributions.** KM contributed to the data, conceived portion of the study, and
565 performed statistical analysis and drafted the article. ATL, CZL, AH contributed to the data
566 analysis and in computing the epigenetic clocks and predictor. JVS contributed to the lab work.
567 RWW conceived of the BXD Aging Colony, and provided access to the BXD biospecimen and
568 data. SH developed the array platform, and built the epigenetic clocks and predictor. All authors
569 contributed to, and approved the manuscript.

570 **Research funding.** This study was funded by the NIH NIA grants R21AG055841 and
571 R01AG043930

572 **Competing interests.** SH is a founder of the non-profit Epigenetic Clock Development
573 Foundation, which plans to license several of his patents from his employer UC Regents. The
574 other authors declare no conflicts of interest.

575 **Ethics approval.** All animal procedures were in accordance to protocol approved by the
576 Institutional Animal Care and Use Committee (IACUC) at the University of Tennessee Health
577 Science Center.

578 **Reference:**

579 1 Horvath, S. & Raj, K. DNA methylation-based biomarkers and the epigenetic clock theory
580 of ageing. *Nature reviews. Genetics* **19**, 371-384, doi:10.1038/s41576-018-0004-3
581 (2018).
582 2 Zannas, A. S. *et al.* Lifetime stress accelerates epigenetic aging in an urban, African
583 American cohort: relevance of glucocorticoid signaling. *Genome biology* **16**, 266,
584 doi:10.1186/s13059-015-0828-5 (2015).
585 3 Marioni, R. E. *et al.* The epigenetic clock is correlated with physical and cognitive fitness
586 in the Lothian Birth Cohort 1936. *International journal of epidemiology* **44**, 1388-1396,
587 doi:10.1093/ije/dyu277 (2015).
588 4 Dugue, P. A. *et al.* DNA methylation-based biological aging and cancer risk and survival:
589 Pooled analysis of seven prospective studies. *Int J Cancer* **142**, 1611-1619,
590 doi:10.1002/ijc.31189 (2018).
591 5 Lu, A. T. *et al.* DNA methylation GrimAge strongly predicts lifespan and healthspan.
592 *Aging* **11**, 303-327, doi:10.18632/aging.101684 (2019).
593 6 Ryan, J., Wrigglesworth, J., Loong, J., Fransquet, P. D. & Woods, R. L. A systematic review
594 and meta-analysis of environmental, lifestyle and health factors associated with DNA
595 methylation age. *The journals of gerontology. Series A, Biological sciences and medical*
596 *sciences*, doi:10.1093/gerona/glz099 (2019).
597 7 Hannum, G. *et al.* Genome-wide methylation profiles reveal quantitative views of
598 human aging rates. *Molecular cell* **49**, 359-367, doi:10.1016/j.molcel.2012.10.016
599 (2013).
600 8 Horvath, S. DNA methylation age of human tissues and cell types. *Genome biology* **14**,
601 R115, doi:10.1186/gb-2013-14-10-r115 (2013).
602 9 Petkovich, D. A. *et al.* Using DNA Methylation Profiling to Evaluate Biological Age and
603 Longevity Interventions. *Cell metabolism* **25**, 954-960 e956,
604 doi:10.1016/j.cmet.2017.03.016 (2017).
605 10 Stubbs, T. M. *et al.* Multi-tissue DNA methylation age predictor in mouse. *Genome*
606 *biology* **18**, 68, doi:10.1186/s13059-017-1203-5 (2017).
607 11 Wang, T. *et al.* Epigenetic aging signatures in mice livers are slowed by dwarfism, calorie
608 restriction and rapamycin treatment. *Genome biology* **18**, 57, doi:10.1186/s13059-017-
609 1186-2 (2017).
610 12 Horvath, S. *et al.* Epigenetic clock for skin and blood cells applied to Hutchinson Gilford
611 Progeria Syndrome and ex vivo studies. *Aging* **10**, 1758-1775,
612 doi:10.18632/aging.101508 (2018).

613 13 Levine, M. E. *et al.* An epigenetic biomarker of aging for lifespan and healthspan. *Aging*
614 **10**, 573-591, doi:10.18632/aging.101414 (2018).
615 14 Shireby, G. L. *et al.* Recalibrating the epigenetic clock: implications for assessing
616 biological age in the human cortex. *Brain* **143**, 3763-3775, doi:10.1093/brain/awaa334
617 (2020).
618 15 Arneson, A. *et al.* A mammalian methylation array for profiling methylation levels at
619 conserved sequences. *bioRxiv*, 2021.2001.2007.425637, doi:10.1101/2021.01.07.425637
620 (2021).
621 16 Lu, A. T. *et al.* Universal DNA methylation age across mammalian tissues. *bioRxiv*,
622 2021.2001.2018.426733, doi:10.1101/2021.01.18.426733 (2021).
623 17 Li, C. Z. *et al.* Epigenetic predictors of maximum lifespan and other life history traits in
624 mammals. *bioRxiv*, 2021.2005.2016.444078, doi:10.1101/2021.05.16.444078 (2021).
625 18 Roy, S. *et al.* Gene-by-environmental modulation of longevity and weight gain in the
626 murine BXD family. *bioRxiv*, 776559, doi:10.1101/776559 (2020).
627 19 Williams, E. G. *et al.* Multi-Omic Profiling of the Liver Across Diets and Age in a Diverse
628 Mouse Population. *bioRxiv*, 2020.2008.2020.222968, doi:10.1101/2020.08.20.222968
629 (2020).
630 20 Ashbrook, D. G. *et al.* A Platform for Experimental Precision Medicine: The Extended
631 BXD Mouse Family. *Cell Syst*, doi:10.1016/j.cels.2020.12.002 (2021).
632 21 Peirce, J. L., Lu, L., Gu, J., Silver, L. M. & Williams, R. W. A new set of BXD recombinant
633 inbred lines from advanced intercross populations in mice. *BMC genetics* **5**, 7,
634 doi:10.1186/1471-2156-5-7 (2004).
635 22 de Haan, G. & Williams, R. W. A genetic and genomic approach to identify longevity
636 genes in mice. *Mechanisms of ageing and development* **126**, 133-138,
637 doi:10.1016/j.mad.2004.09.012 (2005).
638 23 Hsu, H. C. *et al.* Age-related thymic involution in C57BL/6J x DBA/2J recombinant-inbred
639 mice maps to mouse chromosomes 9 and 10. *Genes and immunity* **4**, 402-410,
640 doi:10.1038/sj.gene.6363982 (2003).
641 24 Lang, D. H. *et al.* Quantitative trait loci (QTL) analysis of longevity in C57BL/6J by DBA/2J
642 (BXD) recombinant inbred mice. *Aging clinical and experimental research* **22**, 8-19
643 (2010).
644 25 Sandoval-Sierra, J. V. *et al.* Body weight and high-fat diet are associated with epigenetic
645 aging in female members of the BXD murine family. *Aging cell*, e13207,
646 doi:10.1111/acel.13207 (2020).
647 26 Gibson, J. *et al.* A meta-analysis of genome-wide association studies of epigenetic age
648 acceleration. *PLoS genetics* **15**, e1008104, doi:10.1371/journal.pgen.1008104 (2019).
649 27 Lu, A. T. *et al.* GWAS of epigenetic aging rates in blood reveals a critical role for TERT.
650 *Nature communications* **9**, 387, doi:10.1038/s41467-017-02697-5 (2018).
651 28 McCartney, D. L. *et al.* Genome-wide association studies identify 137 loci for DNA
652 methylation biomarkers of ageing. *bioRxiv*, 2020.2006.2029.133702,
653 doi:10.1101/2020.06.29.133702 (2020).
654 29 Benton, M. C. *et al.* Methylome-wide association study of whole blood DNA in the
655 Norfolk Island isolate identifies robust loci associated with age. *Aging* **9**, 753-768,
656 doi:10.18632/aging.101187 (2017).

30 Yashin, A. I. *et al.* Genetics of Human Longevity From Incomplete Data: New Findings From the Long Life Family Study. *The journals of gerontology. Series A, Biological sciences and medical sciences* **73**, 1472-1481, doi:10.1093/gerona/gly057 (2018).
31 Zhou, X. & Stephens, M. Efficient multivariate linear mixed model algorithms for genome-wide association studies. *Nature methods* **11**, 407-409, doi:10.1038/nmeth.2848 (2014).
32 Peirce, J. L., Broman, K. W., Lu, L. & Williams, R. W. A simple method for combining genetic mapping data from multiple crosses and experimental designs. *PloS one* **2**, e1036, doi:10.1371/journal.pone.0001036 (2007).
33 Catalog, G. <https://www.ebi.ac.uk/gwas/> (
34 Horvath, S. *et al.* Obesity accelerates epigenetic aging of human liver. *Proceedings of the National Academy of Sciences of the United States of America* **111**, 15538-15543, doi:10.1073/pnas.1412759111 (2014).
35 Nevalainen, T. *et al.* Obesity accelerates epigenetic aging in middle-aged but not in elderly individuals. *Clinical epigenetics* **9**, 20, doi:10.1186/s13148-016-0301-7 (2017).
36 Xie, H. *et al.* Genome-wide quantitative assessment of variation in DNA methylation patterns. *Nucleic acids research* **39**, 4099-4108, doi:10.1093/nar/gkr017 (2011).
37 Hayflick, L. Entropy explains aging, genetic determinism explains longevity, and undefined terminology explains misunderstanding both. *PLoS genetics* **3**, e220, doi:10.1371/journal.pgen.0030220 (2007).
38 Lu, A. T. *et al.* Universal DNA methylation age across mammalian tissues. *bioRxiv*, 2021.2001.2018.426733, doi:10.1101/2021.01.18.426733 (2021).
39 Holman, G. D. A new deadly Syn? *Curr Biol* **9**, R735-737, doi:10.1016/s0960-9822(99)80471-0 (1999).
40 Michailidou, K. *et al.* Association analysis identifies 65 new breast cancer risk loci. *Nature* **551**, 92-94, doi:10.1038/nature24284 (2017).
41 Rokudai, S. *et al.* STXBP4 regulates APC/C-mediated p63 turnover and drives squamous cell carcinogenesis. *Proceedings of the National Academy of Sciences of the United States of America* **115**, E4806-E4814, doi:10.1073/pnas.1718546115 (2018).
42 Kichaev, G. *et al.* Leveraging Polygenic Functional Enrichment to Improve GWAS Power. *American journal of human genetics* **104**, 65-75, doi:10.1016/j.ajhg.2018.11.008 (2019).
43 Perry, J. R. *et al.* Parent-of-origin-specific allelic associations among 106 genomic loci for age at menarche. *Nature* **514**, 92-97, doi:10.1038/nature13545 (2014).
44 Albertsen, H. M. *et al.* A physical map and candidate genes in the BRCA1 region on chromosome 17q12-21. *Nature genetics* **7**, 472-479, doi:10.1038/ng0894-472 (1994).
45 Kauraniemi, P. & Kallioniemi, A. Activation of multiple cancer-associated genes at the ERBB2 amplicon in breast cancer. *Endocr Relat Cancer* **13**, 39-49, doi:10.1677/erc.1.01147 (2006).
46 Tanaka, S. *et al.* Coexpression of Grb7 with epidermal growth factor receptor or Her2/erbB2 in human advanced esophageal carcinoma. *Cancer research* **57**, 28-31 (1997).
47 de Vries, P. S. *et al.* Multiancestry Genome-Wide Association Study of Lipid Levels Incorporating Gene-Alcohol Interactions. *Am J Epidemiol* **188**, 1033-1054, doi:10.1093/aje/kwz005 (2019).

701 48 Richardson, T. G. *et al.* Evaluating the relationship between circulating lipoprotein lipids
702 and apolipoproteins with risk of coronary heart disease: A multivariable Mendelian
703 randomisation analysis. *PLoS Med* **17**, e1003062, doi:10.1371/journal.pmed.1003062
704 (2020).
705 49 Xu, Y. *et al.* IKK interacts with rictor and regulates mTORC2. *Cell Signal* **25**, 2239-2245,
706 doi:10.1016/j.cellsig.2013.07.008 (2013).
707 50 Gallagher, M. D. & Chen-Plotkin, A. S. The Post-GWAS Era: From Association to Function.
708 *American journal of human genetics* **102**, 717-730, doi:10.1016/j.ajhg.2018.04.002
709 (2018).
710 51 Lappalainen, T. Functional genomics bridges the gap between quantitative genetics and
711 molecular biology. *Genome research* **25**, 1427-1431, doi:10.1101/gr.190983.115 (2015).
712 52 Olona, A. *et al.* Epoxygenase inactivation exacerbates diet and aging-associated
713 metabolic dysfunction resulting from impaired adipogenesis. *Mol Metab* **11**, 18-32,
714 doi:10.1016/j.molmet.2018.03.003 (2018).
715 53 Schuck, R. N. *et al.* The cytochrome P450 epoxygenase pathway regulates the hepatic
716 inflammatory response in fatty liver disease. *PloS one* **9**, e110162,
717 doi:10.1371/journal.pone.0110162 (2014).
718 54 Wang, Q. *et al.* Time serial transcriptome reveals Cyp2c29 as a key gene in
719 hepatocellular carcinoma development. *Cancer Biol Med* **17**, 401-417,
720 doi:10.20892/j.issn.2095-3941.2019.0335 (2020).
721 55 Mozhui, K. *et al.* Dissection of a QTL hotspot on mouse distal chromosome 1 that
722 modulates neurobehavioral phenotypes and gene expression. *PLoS genetics* **4**,
723 e1000260, doi:10.1371/journal.pgen.1000260 (2008).
724 56 Zhou, W., Triche, T. J., Jr., Laird, P. W. & Shen, H. SeSAMe: reducing artifactual detection
725 of DNA methylation by Infinium BeadChips in genomic deletions. *Nucleic acids research*
726 **46**, e123, doi:10.1093/nar/gky691 (2018).
727 57 Haghani, A. *et al.* DNA Methylation Networks Underlying Mammalian Traits. *bioRxiv*,
728 2021.2003.2016.435708, doi:10.1101/2021.03.16.435708 (2021).
729 58 Hausser, J. & Strimmer, K. Entropy Inference and the James-Stein Estimator, with
730 Application to Nonlinear Gene Association Networks. *J. Mach. Learn. Res.* **10**, 1469–
731 1484 (2009).
732 59 *GeneNetwork 2*, <http://genenetwork.org> (
733 60 Ashbrook, D. G. *et al.* Born to Cry: A Genetic Dissection of Infant Vocalization. *Front*
734 *Behav Neurosci* **12**, 250, doi:10.3389/fnbeh.2018.00250 (2018).
735 61 Belknap, J. K. Effect of within-strain sample size on QTL detection and mapping using
736 recombinant inbred mouse strains. *Behavior genetics* **28**, 29-38 (1998).
737 62 Sherry, S. T. *et al.* dbSNP: the NCBI database of genetic variation. *Nucleic acids research*
738 **29**, 308-311, doi:10.1093/nar/29.1.308 (2001).
739 63 Bates, D., Maechler, M., Bolker, B. & Walker, S. lme4: Linear mixed-effects models using
740 Eigen and S4. . *R package version 1.1-7, http://CRAN.R-project.org/package=lme4*.
741 64 *Wellcome Sanger Institute Mouse Genome Project*,
742 <https://www.sanger.ac.uk/sanger/Mouse_SnpViewer/rel-1505> (
743 65 Keane, T. M. *et al.* Mouse genomic variation and its effect on phenotypes and gene
744 regulation. *Nature* **477**, 289-294, doi:10.1038/nature10413 (2011).

745 66 Yalcin, B. *et al.* Sequence-based characterization of structural variation in the mouse
746 genome. *Nature* **477**, 326-329, doi:10.1038/nature10432 (2011).
747 67 Huang da, W., Sherman, B. T. & Lempicki, R. A. Bioinformatics enrichment tools: paths
748 toward the comprehensive functional analysis of large gene lists. *Nucleic acids research*
749 **37**, 1-13, doi:10.1093/nar/gkn923 (2009).
750 68 Huang da, W., Sherman, B. T. & Lempicki, R. A. Systematic and integrative analysis of
751 large gene lists using DAVID bioinformatics resources. *Nature protocols* **4**, 44-57,
752 doi:10.1038/nprot.2008.211 (2009).
753

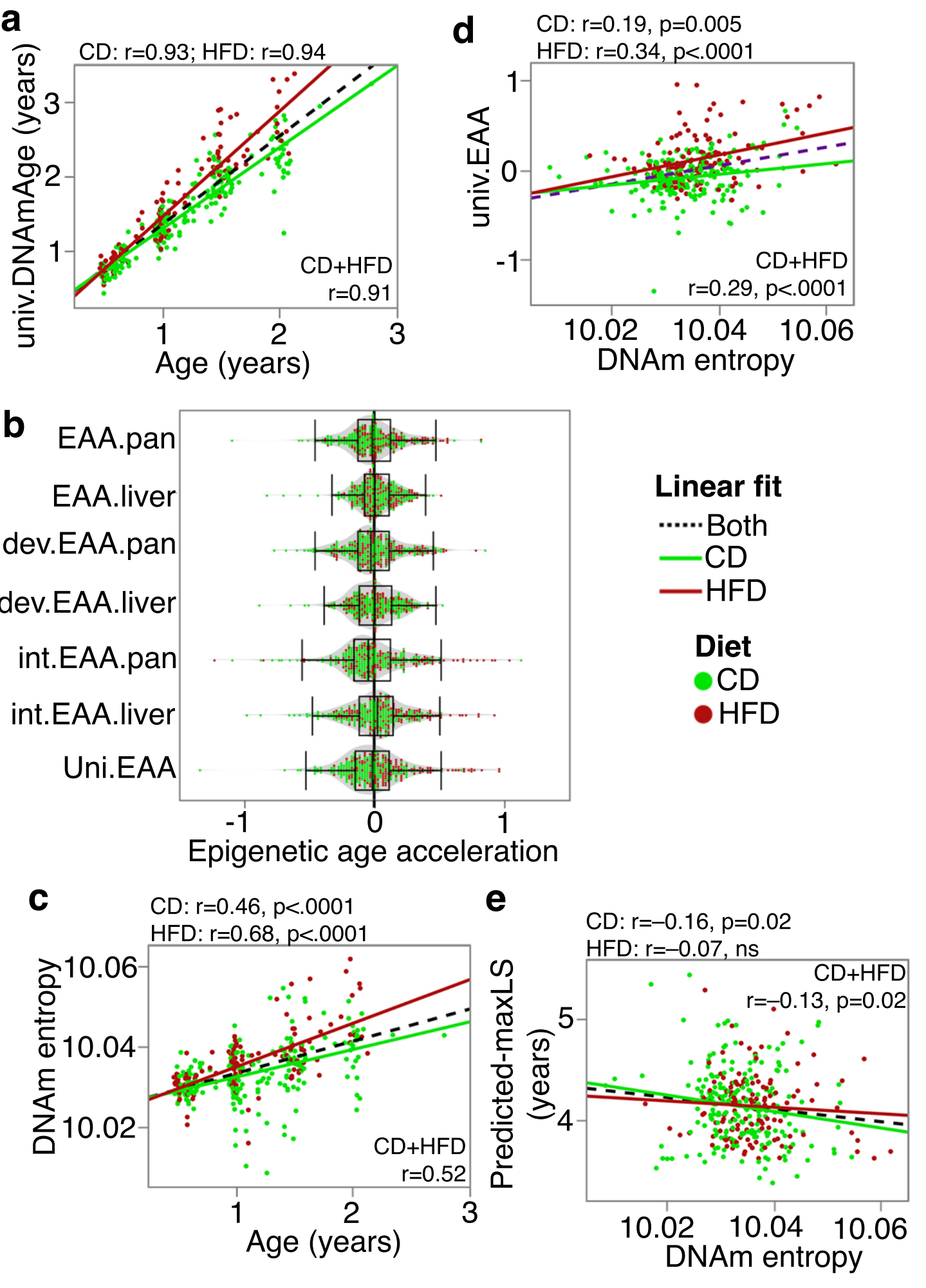
a
CD: r=0.93; HFD: r=0.94
univ.DNAmAge (years)
CD+HFD
r=0.91
Age (years)
d
CD: r=0.19, p=0.005
HFD: r=0.34, p<.0001
univ.EAA
CD+HFD
r=0.29, p<.0001
DNAm entropy
b
EAA.pan
EAA.liver
dev.EAA.pan
dev.EAA.liver
int.EAA.pan
int.EAA.liver
Uni.EAA
Epigenetic age acceleration
Linear fit
Both
CD
HFD
Diet
CD
HFD
c
CD: r=0.46, p<.0001
HFD: r=0.68, p<.0001
DNAm entropy
CD+HFD
r=0.52
Age (years)
e
CD: r=–0.16, p=0.02
HFD: r=–0.07, ns
Predicted-maxLS (years)
CD+HFD
r=–0.13, p=0.02
DNAm entropy

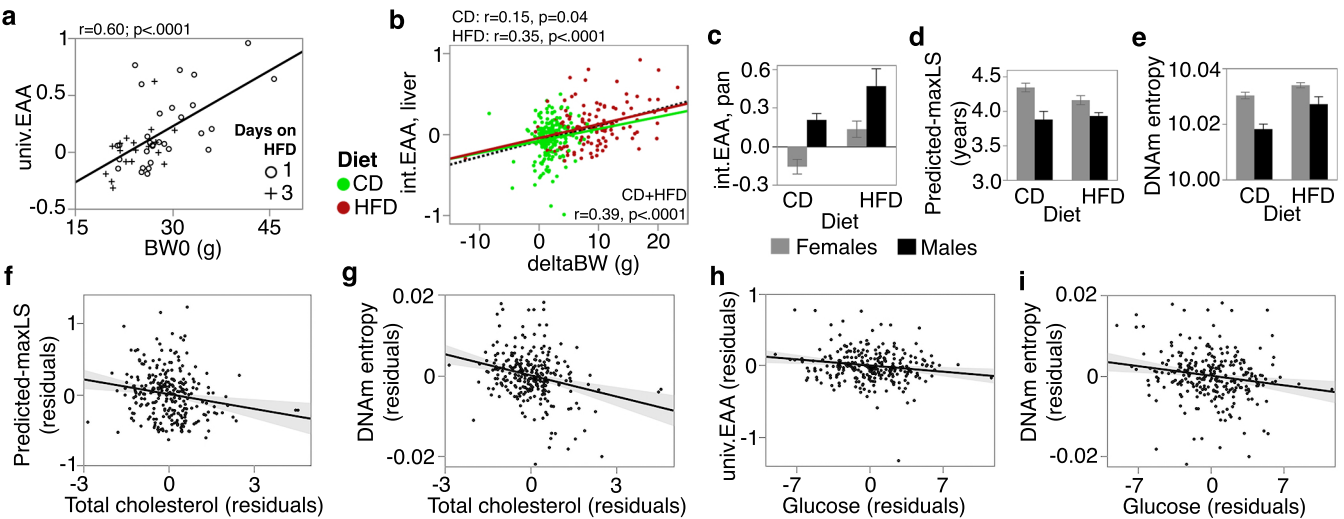
a
r=0.60; p<.0001
univ.EAA
BW0 (g)
Days on HFD
○ 1
+ 3
b
CD: r=0.15, p=0.04
HFD: r=0.35, p<.0001
int.EAA, liver
deltaBW (g)
Diet
CD
HFD
CD+HFD
r=0.39, p<.0001
c
int.EAA, pan
CD
HFD
Diet
Females
Males
d
Predicted-maxLS (years)
CD
HFD
Diet
e
DNAm entropy
CD
HFD
Diet
f
Predicted-maxLS (residuals)
Total cholesterol (residuals)
g
DNAm entropy (residuals)
Total cholesterol (residuals)
h
univ.EAA (residuals)
Glucose (residuals)
i
DNAm entropy (residuals)
Glucose (residuals)

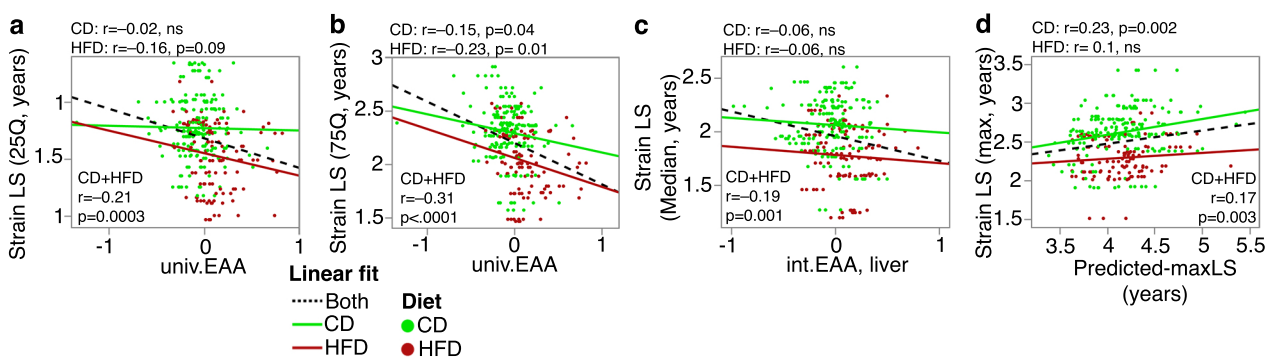
a
CD: r=−0.02, ns
HFD: r=−0.16, p=0.09
Strain LS (25Q, years)
CD+HFD
r=−0.21
p=0.0003
univ.EAA
b
CD: r=−0.15, p=0.04
HFD: r=−0.23, p= 0.01
Strain LS (75Q, years)
CD+HFD
r=−0.31
p<.0001
univ.EAA
c
CD: r=−0.06, ns
HFD: r=−0.06, ns
Strain LS (Median, years)
CD+HFD
r=−0.19
p=0.001
int.EAA, liver
d
CD: r=0.23, p=0.002
HFD: r= 0.1, ns
Strain LS (max, years)
CD+HFD
r=0.17
p=0.003
Predicted-maxLS (years)
Linear fit
Both
CD
HFD
Diet
CD
HFD

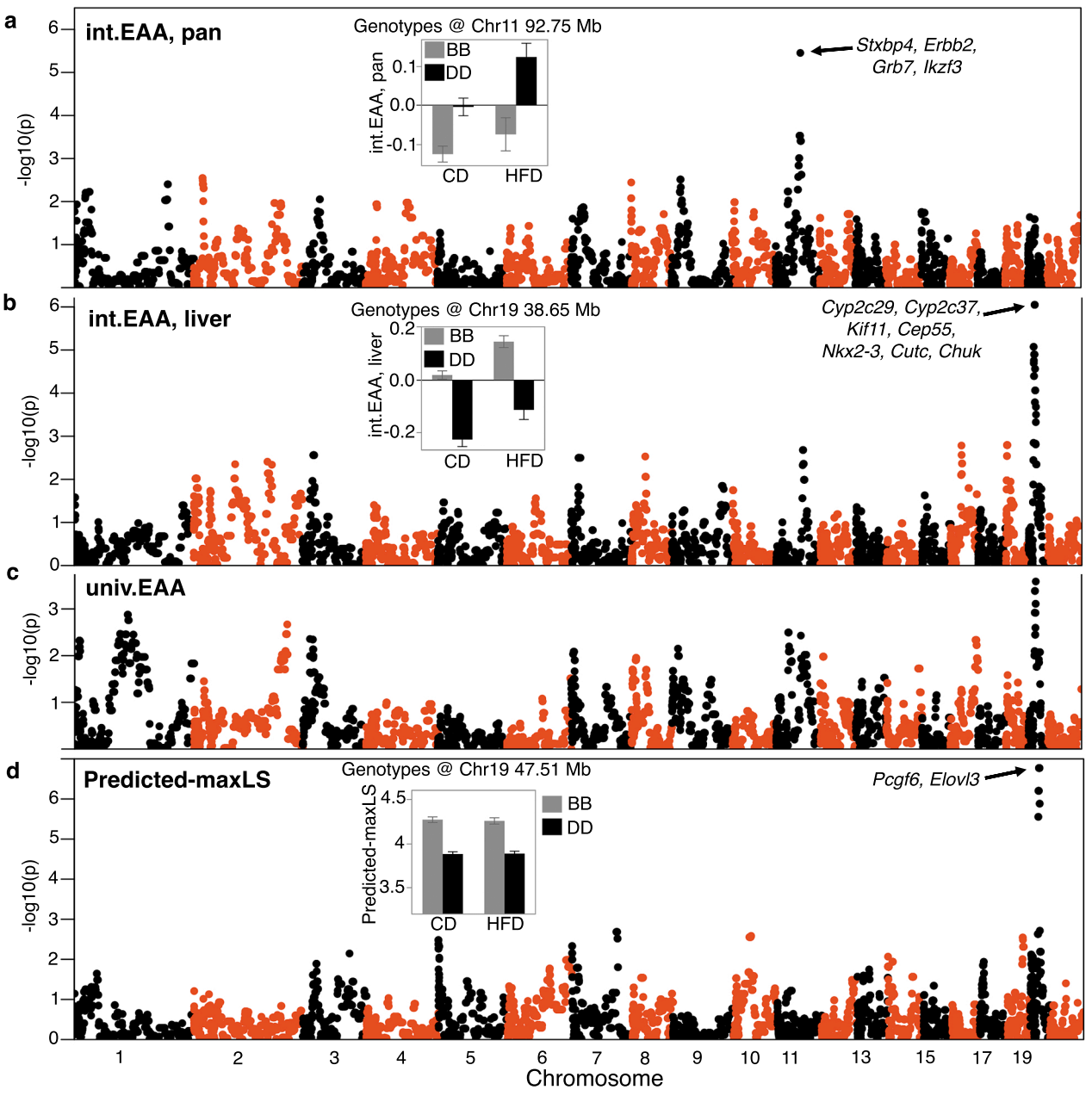
a
int.EAA, pan
Genotypes @ Chr11 92.75 Mb
BB
DD
int.EAA, pan
0.1
0.0
-0.1
CD
HFD
Stxbp4, Erbb2,
Grb7, Ikzf3
-log10(p)
b
int.EAA, liver
Genotypes @ Chr19 38.65 Mb
BB
DD
int.EAA, liver
0.2
0.0
-0.2
CD
HFD
Cyp2c29, Cyp2c37,
Kif11, Cep55,
Nkx2-3, Cutc, Chuk
-log10(p)
c
univ.EAA
-log10(p)
d
Predicted-maxLS
Genotypes @ Chr19 47.51 Mb
BB
DD
Predicted-maxLS
4.5
4
3.5
CD
HFD
Pcgf6, Elovl3
-log10(p)
1
2
3
4
5
6
7
8
9
10
11
13
15
17
19
Chromosome

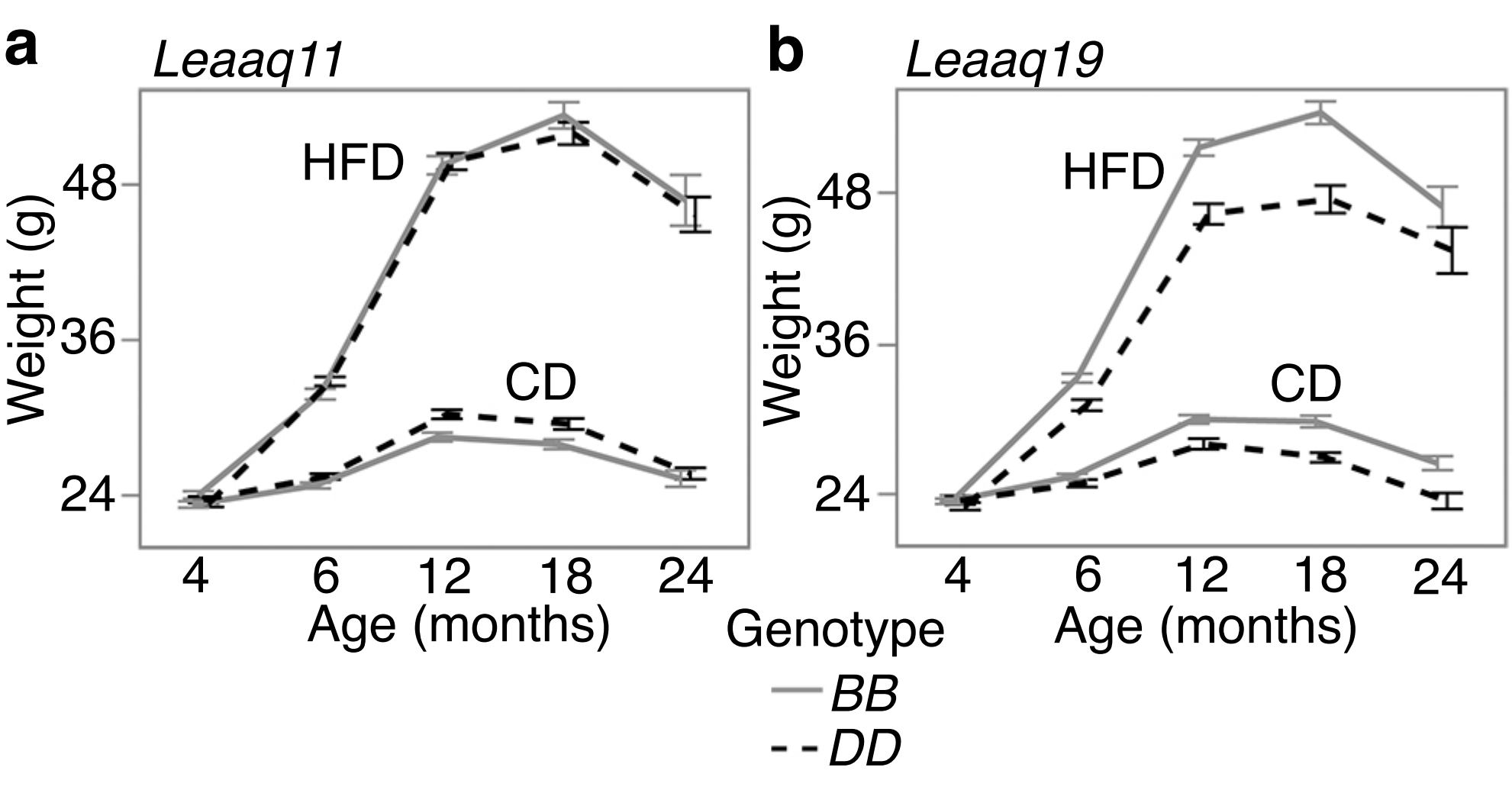
a
Leaaq11
HFD
CD
Weight (g)
48
36
24
4
6
12
18
24
Age (months)
b
Leaaq19
HFD
CD
Weight (g)
48
36
24
4
6
12
18
24
Age (months)
Genotype
BB
DD

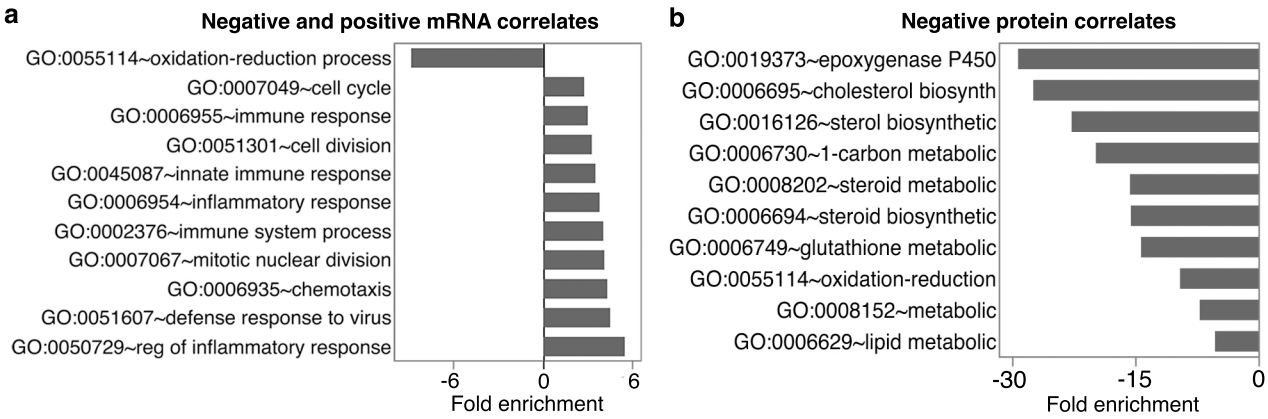
a
Negative and positive mRNA correlates
GO:0055114~oxidation-reduction process
GO:0007049~cell cycle
GO:0006955~immune response
GO:0051301~cell division
GO:0045087~innate immune response
GO:0006954~inflammatory response
GO:0002376~immune system process
GO:0007067~mitotic nuclear division
GO:0006935~chemotaxis
GO:0051607~defense response to virus
GO:0050729~reg of inflammatory response
-6
0
6
Fold enrichment
b
Negative protein correlates
GO:0019373~epoxygenase P450
GO:0006695~cholesterol biosynth
GO:0016126~sterol biosynthetic
GO:0006730~1-carbon metabolic
GO:0008202~steroid metabolic
GO:0006694~steroid biosynthetic
GO:0006749~glutathione metabolic
GO:0055114~oxidation-reduction
GO:0008152~metabolic
GO:0006629~lipid metabolic
-30
-15
0
Fold enrichment